The use of charge extraction by linearly increasing voltage in polar organic light-emitting diodes

Simon Züfle,[1,2,a)] Stéphane Altazin,[2] Alexander Hofmann,[3] Lars Jäger,[3]
Martin T. Neukom,[1,2] Tobias D. Schmidt,[3] Wolfgang Brütting,[3] and Beat Ruhstaller[1,2]
[1]*Institute of Computational Physics, Zurich University of Applied Sciences, Technikumstr. 9, 8401 Winterthur, Switzerland*
[2]*Fluxim AG, Technoparkstr. 2, 8406 Winterthur, Switzerland*
[3]*Institute of Physics, University of Augsburg, 86135 Augsburg, Germany*

(Received 12 January 2017; accepted 1 April 2017; published online 4 May 2017)

We demonstrate the application of the CELIV (charge carrier extraction by linearly increasing voltage) technique to bilayer organic light-emitting devices (OLEDs) in order to selectively determine the hole mobility in N,N0-bis(1-naphthyl)-N,N0-diphenyl-1,10-biphenyl-4,40-diamine (α-NPD). In the CELIV technique, mobile charges in the active layer are extracted by applying a negative voltage ramp, leading to a peak superimposed to the measured displacement current whose temporal position is related to the charge carrier mobility. In fully operating devices, however, bipolar carrier transport and recombination complicate the analysis of CELIV transients as well as the assignment of the extracted mobility value to one charge carrier species. This has motivated a new approach of fabricating dedicated metal-insulator-semiconductor (MIS) devices, where the extraction current contains signatures of only one charge carrier type. In this work, we show that the MIS-CELIV concept can be employed in bilayer polar OLEDs as well, which are easy to fabricate using most common electron transport layers (ETLs), like Tris-(8-hydroxyquinoline)aluminum (Alq_3). Due to the macroscopic polarization of the ETL, holes are already injected into the hole transport layer below the built-in voltage and accumulate at the internal interface with the ETL. This way, by a standard CELIV experiment only holes will be extracted, allowing us to determine their mobility. The approach can be established as a powerful way of selectively measuring charge mobilities in new materials in a standard device configuration. © *2017 Author(s). All article content, except where otherwise noted, is licensed under a Creative Commons Attribution (CC BY) license (http://creativecommons.org/licenses/by/4.0/).* [http://dx.doi.org/10.1063/1.4982903]

I. INTRODUCTION

Charge carrier mobility is one of the most important material parameters in organic electronics. In organic light-emitting diodes (OLEDs) where electrons and holes are injected by electrodes and recombine in the active layer, leading to light emission, one of the key factors determining the (current-to-luminance) efficiency is the charge balance factor.[1–3] This factor can be maximized by the stack design, e.g., using blocking layers, as well as optimizing the carrier mobilities in the charge transport layers. Bimolecular carrier recombination is directly proportional to carrier mobility;[4] thus, a high carrier mobility translates into a high recombination efficiency which in turn is linked to a high charge balance factor, too.

In organic solar cells (OSCs), conversely, a high current collection efficiency is based on high carrier mobilities and ensures maximum photocurrent, and low bimolecular recombination losses allow for a high fill factor. As a rule-of-thumb, higher and balanced electron and hole mobilities are favourable for good organic solar cells.[5,6] It has however been shown that there is a trade-off discouraging too high mobilities, and furthermore, monomolecular recombination can play a role as well.[7–9]

In any case, the charge carrier mobility of the majority charge carriers in an organic semiconductor material is one of the most relevant parameters for further optimization of organic electronic devices. Various experimental techniques such as space-charge limited current-voltage curves,[10] time-of-flight,[11,12] admittance spectroscopy,[13,14] dark injection transients,[15,16] field-effect mobility,[17] and charge extraction by linearly increasing voltage (CELIV)[18,19] are in principle available to assess this parameter. Most of these techniques come with the need to fabricate dedicated devices with especially thick layers, or with different contact materials than in the final device geometry to ensure unipolar transport. The only one that can be performed on fully operating devices is photo-CELIV in organic solar cells, where the identification of the sign of the majority charge carrier is a non-obvious task, however.

The CELIV technique was originally developed by Juška *et al.*[18] to extract the charge carrier drift mobility in thin-film silicon, and has been subsequently applied to doped organic layers[20,21] and to organic photovoltaic cells.[22] The technique can in principle be applied to any kind of device that behaves as a diode, meaning that it needs to be non-injecting under reverse bias conditions. Applying a negative voltage ramp induces a constant displacement current due to the electric field changing linearly with time. In case mobile charges are already present in the device under the

a)Electronic mail: simon.zuefle@zhaw.ch

 © Author(s) 2017.

conditions prior to the voltage ramp, these charges are extracted by the reverse field, and the transit time and number of carriers are linked to an additional current peak on top of the displacement current plateau. The charges being extracted can be equilibrium carriers (induced by electrical dopants), photo-generated carriers, or previously injected carriers. We can thus distinguish among dark-CELIV, photo-CELIV, and injection-CELIV. To clarify the experimental details, we schematically show the voltage and current transients in Fig. 1.

The transient position of the CELIV current peak is related to the charge carrier transit time and, therefore, to the mobility. The first analytical model to calculate the mobility μ was given by Juška *et al*. with[18]

$$\mu = \frac{2d^2}{3\mathcal{A} \cdot t_{max}^2}, \tag{1}$$

where the layer thickness is denoted by d, the voltage ramp is $\mathcal{A} = dV/dt$, and the position of the current maximum is t_{max}.

The application of this formula is, however, very limited, as the underlying assumptions (drift only, uniform charge carrier distribution, no RC-effects) are usually not justified.[23] Several other approaches have therefore been pursued to describe the full transient current, and specifically to quantify the mobility.[24–27] In bipolar devices, the peak consists of both electrons and holes, and it is not possible to unambiguously assign the extracted mobility to one specific charge carrier type. Also, depending on the ratio of the electron and hole mobility as well as the ratio of electron and hole density the extracted mobility can be the faster one, the slower one or an average of the two species. Finally, the peak position and thereby the extracted mobility depend on the relation of the peak height j_{max} to the displacement current plateau j_0, the employed voltage ramp rate, (bipolar) recombination, and the external series resistance[23,25] which further complicates the analysis and can render simple analytical formulas inaccurate. There have been adaptions and extensions to the initial equation, but also these are approximations and valid only in specific cases.[21,22,26] A planar heterojunction organic solar cell represents such a special case, where the identification of the carrier species was supported by a thickness variation of either of the two layers.[28] The most general modelling approach for the bipolar case still is the dual-carrier drift-diffusion model, ideally coupled with a fitting routine, which in the end allows for a real quantitative extraction of both charge carrier mobilities.[23,29,30]

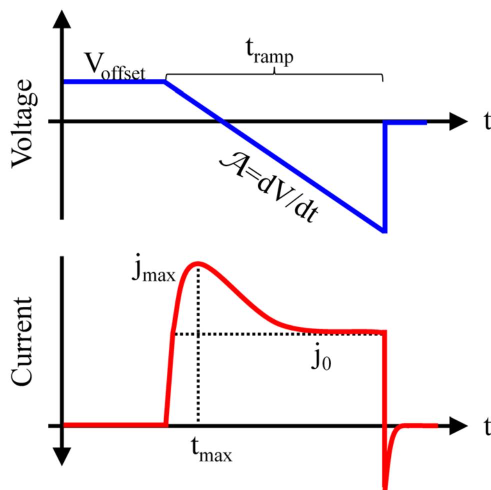

FIG. 1. Schematics of the CELIV experiment, explaining the experimental quantities used in the text.

II. APPROACH

So far, it seemed impossible to use fully operating bipolar devices for a valid CELIV analysis. However, recently several groups have developed a new approach by fabricating metal-insulator-semiconductor (MIS) devices to determine both mobilities of the semiconductor.[9,31,32] Here, the extraction current shows signatures of only one charge carrier type, which was injected in the first place and for which the electrode on the semiconductor is selective. The main advantage of MIS-CELIV is that it is a quite general approach that can be followed for a large range of materials. Furthermore, the active layer to be investigated can be deposited with the same parameters (thickness, morphology) as in the full stack, so the mobilities in the "real" device can be inferred to be very similar. However, the fabrication of well-controlled thin and dense insulating layers can be challenging. The deposition of metal-oxide insulators can harm the underlying organic layer; furthermore, the use of specific insulators like MgF_2 can lead to undesired side effects such as contamination of the evaporation chamber. Finally, interface states between the insulator and organic layer may lead to band-bending and trapping effects and therefore complicate the analysis. These shortcomings render the use of inorganic insulators not suitable for all research groups and every material of interest.

Due to their diode behaviour, OLEDs are also suitable for CELIV experiments but a pre-bias above the built-in potential needs to be applied for injecting carriers in the first place. Like in bulk heterojunction OSCs, the CELIV peak, however, cannot unambiguously be assigned to one carrier type alone as both of them are injected above the built-in voltage. In this work, we present for the first time the application of the CELIV technique in OLEDs with clear identification of the carrier type, namely, holes. For this endeavour, we take advantage of the concept of polar layers.[33,34]

The most simple OLED configuration is a bilayer stack consisting of a hole transport layer (HTL) and an electron transport layer (ETL), sandwiched between the electrodes, where one or both of the two layers shows electroluminescent behaviour such as in the original small molecule OLED structure by Tang and van Slyke.[35] Radiative recombination takes place in the emissive layer at the HTL/ETL interface, as soon as the applied voltage is large enough ($>V_{bi}$) to inject both charge carrier species into their respective transport layers. The most commonly used electron transport materials for OLEDs, like Alq_3, TPBi, BCP, and BPhen,[36,37] exhibit a permanent macroscopic polarization due to spontaneous orientation of molecular dipoles upon layer deposition, forming an effective sheet charge density on both sides of

the layer.[38] It has been shown that this polarization effect leads to a reduction of the hole injection voltage V_t, dependent on the thickness of the ETL and on the interface charge density, according to the following equation:[33,34]

$$V_t = V_{bi} + \frac{Q_S d_{ETL}}{\varepsilon_0 \varepsilon_r} = V_{bi} + \frac{Q_S}{C_{ETL}}, \quad (2)$$

where Q_S denotes the effective sheet charge density, d_{ETL} is the thickness, ε_r is the permittivity and C_{ETL} is the capacitance per unit area of the polar ETL, and V_{bi} is the built-in voltage generated by the electrode work function difference. Note that Q_S is negative in most cases leading to V_t smaller than V_{bi}. In fact, with a thick enough ETL the hole injection voltage can be even shifted into the negative bias regime, meaning that below zero bias holes already need to be injected into the HTL in order to reach equilibrium conditions in a closed circuit. Therefore in the voltage range between V_t and V_{bi}, the OLED behaves like a MIS device in the accumulation regime and the MIS-CELIV technique can be employed without the need for an insulating layer and still ensuring carrier selectivity.

III. EXPERIMENTAL

In order to demonstrate the approach proposed here, we investigate a prototypical OLED stack consisting of ITO (160 nm)/PEDOT:PSS(30 nm)/N,N0-bis(1-naphthyl)-N,N0-diphenyl-1,10-biphenyl-4,40-diamine (α-NPD)(80 nm)/Alq_3 (60 nm)/Ca(15 nm)/Al(100 nm). The devices have been fabricated at Augsburg University using standard procedures that have already been described elsewhere.[37] The electrical transient and impedance measurements reported here have been performed by the all-in-one characterization platform Paios developed and commercialized by Fluxim AG, Switzerland.[39] Drift-diffusion simulations to calculate the CELIV currents and charge density profiles have been generated using the commercial tool Setfos 4.4 by Fluxim AG,[40] which was already successfully used to characterize OSCs[23,30,41] and OLEDs.[38,42] Hereby, the macroscopic polarization was taken into account as demonstrated in our previous publication.[38]

IV. RESULTS

In polar OLEDs, the capacitance-voltage curve shows three regimes, as seen in Fig. 2.[34] At high reverse bias, the bilayer device is insulating and the measured capacitance is the geometric capacitance of the complete stack, $C_{geo} = \left(\frac{d_{HTL}}{\varepsilon_0 \varepsilon_{HTL}} + \frac{d_{ETL}}{\varepsilon_0 \varepsilon_{ETL}}\right)^{-1}$. The hole injection voltage V_t (in this case -1.2 V) is identified as the transition voltage where the capacitance increases from this value to the capacitance of the ETL $C_{ETL} = \frac{\varepsilon_0 \varepsilon_{ETL}}{d_{ETL}}$. When holes are injected into the HTL, it does no longer represent an insulating dielectric and therefore does not contribute to the capacitance any more. The third regime is above the built-in voltage, where bipolar charge injection and radiative recombination set in so that the capacitance drops and can even become negative.[43,44] It is noteworthy that the position of the hole injection voltage can also be obtained by a slow "reverse" CELIV or DCM (displacement current measurement), where a positive voltage ramp is applied to the device.[45] As shown in Fig. S1 of the supplementary material the capacitive current response follows the same curve as the capacitance-voltage plot.

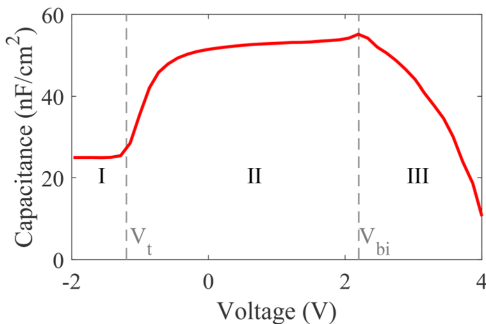

FIG. 2. Capacitance-voltage plot of an α-NPD(80 nm)/Alq_3(60 nm) OLED measured at 100 Hz. The MIS-regime (II) between $V_t = -1.2$ V and $V_{bi} = +2.2$ V is indicated by the vertical dashed lines.

Figures 3(a)–3(c) depict the equilibrium condition of the device at zero volts, that is between V_t and V_{bi}. In the thermodynamic equilibrium at zero volts, one normally expects a negative electric field throughout the device due to the work-function difference of the electrodes. The schematic energy levels in Fig. 3(a) show a large potential drop over the ETL, leading to a strong negative field in this layer caused by the polar sheet charge densities. Conversely, there is a weak positive electric field in the HTL, however, giving rise to hole injection into the HTL. The injected holes accumulate at the internal interface with the polar ETL, since both the interfacial energy barrier and the opposite electric field in the ETL prevent the holes from entering the ETL. This is shown in Fig. 3(b) where we simulate the equilibrium charge density profile inside the bilayer device. Moreover, we show the simulated band diagram for this situation in Fig. 3(c), confirming that there is a driving force for holes to be injected already below V_{bi}.[38]

For comparison, Figs. 3(d)–3(f) show the corresponding situation in a standard MIS device. Here, a forward bias above the built-in potential is applied. The resulting small positive electric field enables hole injection into the HTL. The injected holes accumulate at the HTL/insulator interface, as they cannot overcome the large energetic barrier towards the insulator. Even though the field inside the polar ETL is strongly negative compared to the constant positive field in the insulator, the charge density and potential profile inside the HTL are nearly identical for the two layer stacks. For the simulated electric field profiles and the modeling parameters, we refer to the supplementary material.

Figure 3 proves that a polar OLED in the hole accumulation regime does behave like a standard MIS device under forward bias. Therefore, a CELIV measurement, that is a negative voltage ramp starting from the offset voltage (0 V in Fig. 3), will extract the equilibrium hole density, resulting in the typical extraction peak. In this case, there is no doubt about the type of extracted carriers - holes - and the extracted mobility is neither perturbed by the opposite charge carrier nor by recombination losses.

For the MIS-CELIV measurement, an offset voltage with a value between the hole injection voltage V_t and the

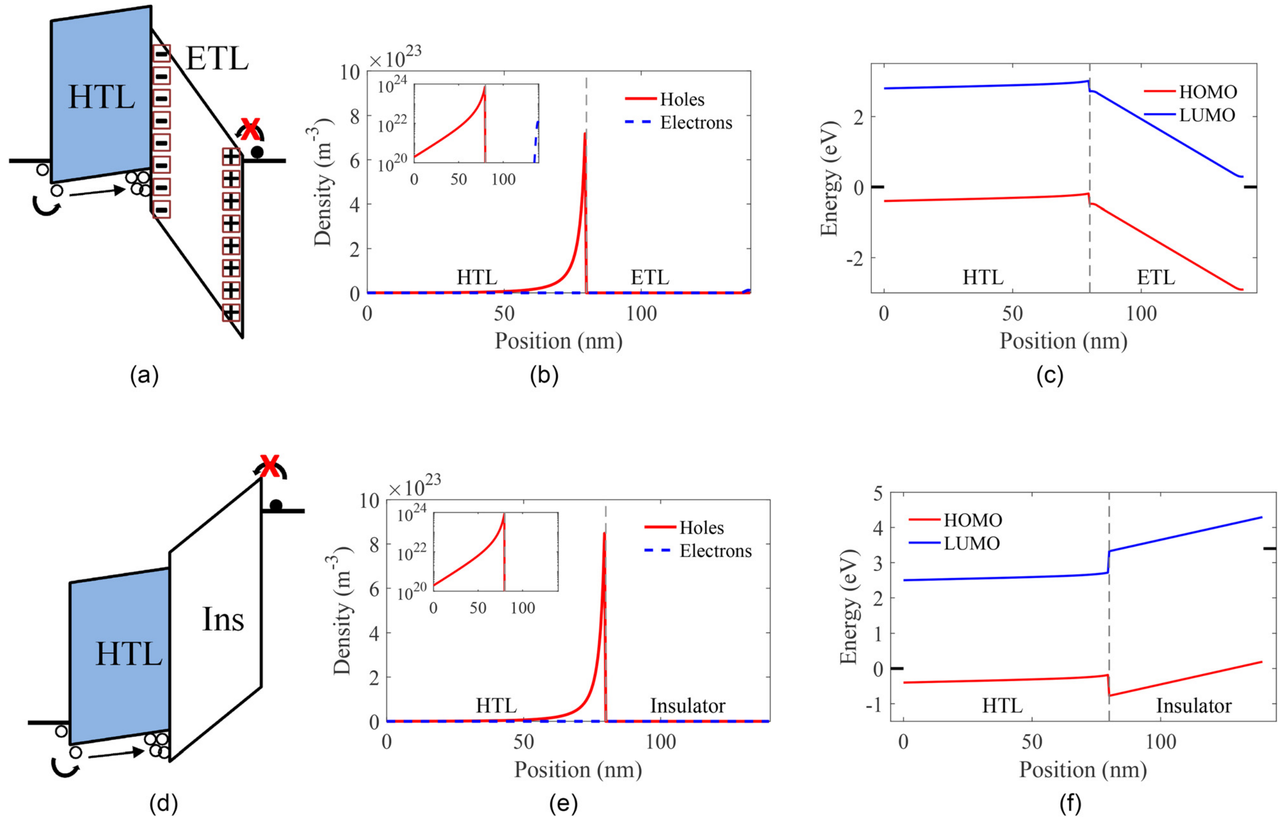

FIG. 3. (a) Schematic energy level diagram of a bilayer OLED with a polar ETL for an offset voltage $V_t < V_{off} < V_{bi}$. The layer under investigation is highlighted by blue colour, the sheet charge densities are denoted by squares, and electrons and holes by filled and open circles, respectively. (b) Simulated equilibrium charge carrier densities of holes (red full line) and electrons (blue dashed line) for an offset voltage of 0 V and using an 80 nm thick HTL (left), a 60 nm thick ETL (right) and assuming a sheet charge density of -1.8 mC/m^2 at the HTL/ETL interface. The inset shows a logarithmic representation. (c) Simulated band diagram for the same layer stack at an offset voltage of 0 V. (d) Schematic energy level diagram of a MIS-device for an offset voltage $V_{off} > V_{bi}$. (e) Simulated equilibrium charge carrier densities of holes (red full line) and electrons (blue dashed line) for an offset voltage of 3.4 V and using an 80 nm thick HTL (left) and a 60 nm thick Insulating layer (right). The inset shows a logarithmic representation. (f) Simulated band diagram for the MIS-device at an offset voltage of 3.4 V.

built-in voltage V_{bi} is applied prior to the CELIV voltage ramp. The closer the offset voltage is to V_{bi}, the more holes will be present in the active layer prior to the extraction ramp. Figure 4 shows the measured CELIV currents using a ramp rate $\mathcal{A} = -2000$ V/ms at varied offset voltages. At offset voltages below the hole injection voltage $V_t = -1.2$ V, both HTL and ETL are empty and therefore insulating. Then, the current density consists only of the displacement current $j_0 = C_{geo} \cdot \mathcal{A}$. For voltages above the hole injection voltage, holes are present prior to the ramp and are extracted by it, leading to the characteristic current peak. We observe a saturation of this peak at a value corresponding to the capacitive current density of the ETL $j_\infty = C_{ETL} \cdot \mathcal{A}$. The appearance of this saturation corresponds to the space-charge limited current, as pointed out by Juška *et al.*[31] The reason is that during a time step not more than the charge on the capacitor plates $C_{ETL} \cdot V$ can be displaced. The ratio of the current levels corresponds to the simple layer thickness ratio $\frac{j_\infty}{j_0} = \frac{d_{ETL} + d_{HTL}}{d_{ETL}}$ of about 2.2 in our case if we neglect differences in dielectric permittivity.

Figure 5 shows various parameters extracted from the data of Fig. 4, which were obtained for an α-NPD/Alq_3 device with offset voltage variation. The current maximum and the extracted charge, which is the time-integrated current $Q_{tot} = \int_0^{t_{ramp}} (j(t) - j_0) dt$, are plotted in Fig. 5(a). Below the hole injection voltage no charges are extracted, and the current is just the constant displacement current. Above V_t holes are extracted, showing up in the linearly rising current maximum and extracted charge. For high voltages above the built-in voltage, both quantities saturate due to the space-charge limitation.

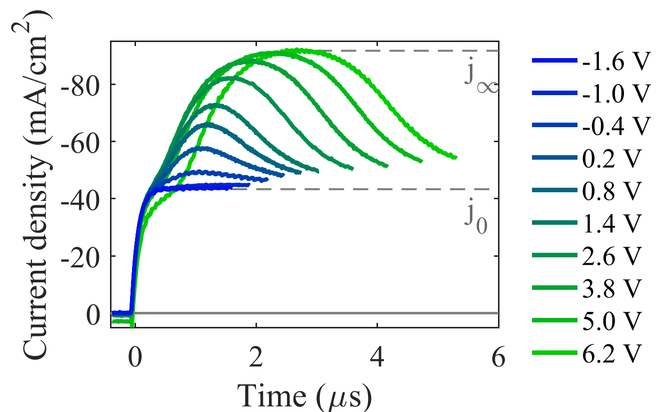

FIG. 4. MIS-CELIV measurement on an α-NPD(80 nm)/Alq_3(60 nm) device at varied offset voltages from -1.6 V to 6.2 V. For offset voltages below the hole injection voltage $V_t = -1.2$ V, only the displacement current plateau is observed. The displacement current j_0 and the saturation current j_∞ are denoted by dashed lines.

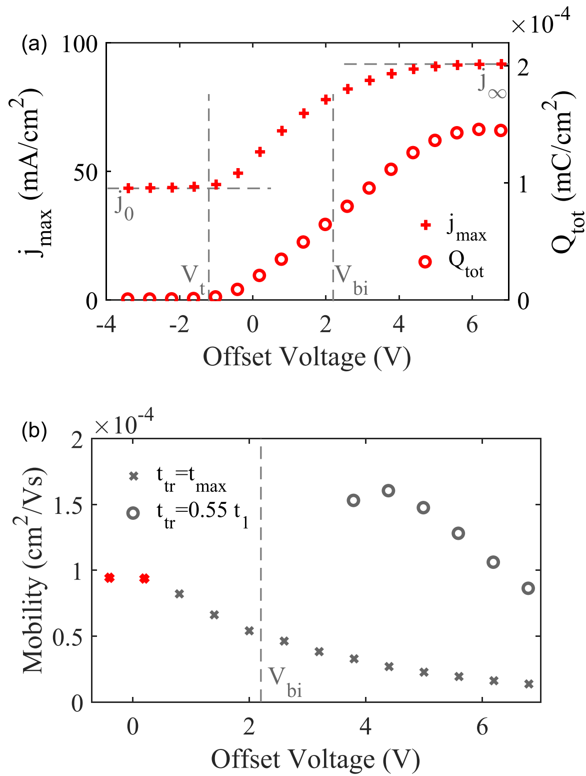

FIG. 5. Extracted parameters from the MIS-CELIV measurements shown in Fig. 4 with offset voltage variation. (a) Current maximum and integrated charge. For clarification, some variables used in the text are also denoted in grey. (b) Calculated mobility using Eq. (3) with two different estimates of the transit time.

In order to determine the hole mobility, the conventional CELIV formula (Eq. (1)) cannot be used as it assumes a bulk charge distribution, and does not account for the redistribution of the electric field by the insulating layer. There is, however, the analytical framework for MIS-CELIV, which was originally proposed by Juška *et al*. This is based on the assumption that all the equilibrium charges accumulate at the internal interface in an infinitesimally narrow distribution[9,31,46]

$$\mu = \frac{2d_{HTL}^2}{\mathcal{A}\cdot t_{tr}^2}\cdot\left(1+\frac{\varepsilon_{HTL}d_{ETL}}{\varepsilon_{ETL}d_{HTL}}\right) = \frac{2d_{HTL}^2}{\mathcal{A}\cdot t_{tr}^2}\cdot\left(1+\frac{j_0}{j_\infty - j_0}\right). \quad (3)$$

In Eq. (3), t_{tr} is the transit time, $\mathcal{A}$ is the voltage ramp, d denotes the layer thicknesses, and ε is the respective relative permittivity of the layers. If the permittivity is not known and the saturation current j_∞ is observed in the measurement, using the second part of Eq. (3) can help to reduce uncertainties.

In standard MIS devices, the ratio j_∞/j_0 is large due to the typically thin insulator layers and their high permittivities. Under this condition, the transit time can be estimated from the time t_1 when the current reaches twice the plateau value, $j(t_1) = 2{\cdot}j_0$.[31] The two times are then related by $t_{tr} = \frac{4}{\pi}\, t_1$.[31,46] In case the proportions of the layer thicknesses are nonideal, Važgėla *et al*. provide a correction factor in Figure 2 of their publication.[46] For our device, the ratio j_∞/j_0 is approximately 2.2, so we take the relation between t_1 and t_{tr} to be approximately: $t_{tr} \approx 0.55 t_1$. The problem is that t_1 can be determined only for high offset voltages above V_{bi}, and hence, the mobility analysis may be disturbed by electron contributions.

Therefore, we focus on the low-conductivity regime by investigating the small peaks that occur for offset voltages just above the hole injection voltage. Here, only a small charge density is present and the extraction current is unperturbed by space-charge effects. In accordance with conventional CELIV theory, Juška *et al.* state that in the small-charge limit the transit time is identical to the transient position of the current peak.[31]

Figure 5(b) shows the extracted mobility values for the measurements of Fig. 4 using Eq. (3). Thereby, we have estimated the transit time by either the peak position $t_{tr} = t_{max}$, or, if possible, using the time t_1 via $t_{tr} = 0.55\ t_1$. The first method gives values around 9×10^{-5} cm^2/Vs just above V_t, while for higher offset voltages the extracted mobility is lower, due to the starting saturation and space-charge effects. The values estimated using t_1 are higher (up to 1.6×10^{-4} cm^2/Vs); however, they are not reliable as t_1 is only observed in the bipolar regime above V_{bi}. We therefore conclude that for bilayer OLEDs the most convenient and reliable way to determine the mobility is from the small-charge regime, that is using offset voltages just above the hole injection voltage.

The extracted values are in qualitative agreement with values reported earlier in the literature: the reported hole mobilities in α-NPD using time-of-flight lie in the range of 3–9×10^{-4} cm^2/Vs,[47–52] values obtained by admittance spectroscopy are 3–4×10^{-4} cm^2/Vs,[51,53] by space-charge limited current 2–90×10^{-5} cm^2/Vs,[54] by field-effect mobility 2×10^{-5} cm^2/Vs,[55] and by dark injection transient currents (DITC) 2×10^{-4} cm^2/Vs.[53] Our own DITC measurements on 1500 nm thick α-NPD films (see the supplementary material) give 2–3×10^{-4} cm^2/Vs at fields on the order of 5×10^4 V/cm.

Obviously, the field dependence can be further investigated, where in the CELIV theory usually the extraction field at the peak time $E_{ext} = \frac{V(t_{tr})-V_{bi}}{d_{tot}}$ is taken. The consistency with mobility values determined by the alternative methods confirms the new CELIV method with standard devices to be reliable in practice.

However, as a side remark we want to note that, instead of using CELIV formulas, we can also resort to drift-diffusion simulations as we have already demonstrated in the context of OSCs.[30,40] Since in the MIS-regime of the polar device only holes are present, the CELIV transients can be fitted with the hole mobility as the only fitting parameter. Using the drift-diffusion simulation software Setfos, we obtain a value of 1.2×10^{-4} cm^2/Vs, in very good agreement with the measurement.

V. DISCUSSION

In principle, the presented approach can also be used in order to analyse the electron mobility of an active layer. In this case, a polar hole transport material is needed, on top of

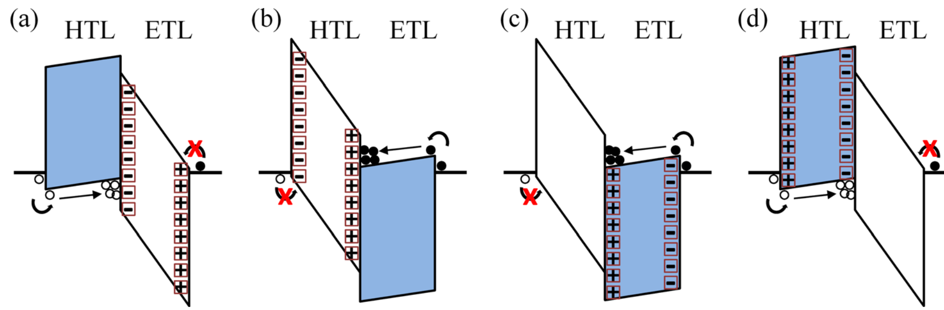

FIG. 6. Schematic energy levels of standard and alternative bilayer configurations of HTL and ETL where one of the layers shows a permanent polar moment, and the layer under investigation is highlighted in blue. The sheet charge densities are denoted by the squares, and mobile electrons, and holes by filled and open circles, respectively. (a) Standard polar OLED configuration as discussed in the main text. The ETL is polar with a negative sheet density at the interface, the hole mobility in the HTL is determined. (b) The HTL is polar with a positive sheet density at the interface. This can be fabricated by dipolar doping of the HTL with a polar material, and can be used to determine the electron mobility in the ETL. (c) The ETL is polar with an inverted polarity. This allows us to determine the electron mobility of the ETL. (d) The HTL is polar with a negative sheet density at the interface. This would allow us to determine the hole mobility of the HTL; however, no such material is reported so far.

which the active layer is deposited, followed by the electron injecting contact (see Fig. 6(b)). While so far no hole transport materials leading to films with a permanent dipole moment have been reported, such materials can be obtained using dipolar doping. Jäger *et al*. have shown that by mixing Alq_3 into an α-NPD matrix the polarity of the HTL can be controlled.[56] The electron transport material Al(7-Prq)$_3$ has been demonstrated by Noguchi *et al*. to exhibit an inverted polarization with a sheet charge density of $+3.1$ mC/m^2.[57] In a bilayer configuration as shown in Fig. 6(c), it would thus be possible to determine the electron mobility in this material. Simulated equilibrium charge and field profiles for this case can also be found in the recent publication by Altazin *et al*.[38] It would then also be feasible that by dipolar doping of Al(7-Prq)$_3$ into an HTL the hole mobility of the HTL host could be determined (Fig. 6(d)).

Of the different configurations depicted in Fig. 6, the first two seem the most relevant, as they allow to selectively determine the hole and electron mobility of an active layer by fabricating two devices where the material under investigation once is deposited onto the hole-injecting contact, and once an electron-selective contact is deposited onto this layer. Obviously, this also allows us to selectively investigate charge carrier transport in general bipolar and bulk-heterojunction semiconductor layers.

Concerning material choice of the polar layer, many commonly used electron transport materials show the orientation polarization effect. In Alq_3, the polar sheet density has been reported by several groups to lie around -1.1 mC/m^2—with the negative polarity at the HTL/ETL interface—confirmed by displacement current measurement,[58,59] capacitance-voltage,[34] and Kelvin Probe[36,60] techniques. For the device reported in Figs. 2 and 4, we find a larger value of $Q_S = -1.8$ mC/m^2 using Eq. (2), which is in agreement with a recent publication by Jäger *et al*. (-1.7 mC/m^2).[56] Obviously, the fabrication conditions play a role in the formation of the macroscopic polarization. Other polar electron transport materials exhibiting orientation polarization are TPBi (-1.1 mC/m^2), BCP, (-0.51 mC/m^2), and OXD-7 (-2.3 mC/m^2).[36]

There are two key advantages of the presented approach compared to other measurement techniques. First, the active layers to be investigated can be prepared and deposited in the same way and especially with the same thickness as in a regular OLED or solar cell stack; thus, the extracted mobility values can be assumed to be the same in the regular device.

The second key advantage is that the employed organic polar electron transport layers are very easy to handle and deposit, and furthermore less harmful to the underlying materials than oxide insulators. Basically every group working in the OLED field can fabricate Alq_3 layers by thermal evaporation, and could thus employ the new CELIV technique.

VI. SUMMARY

We presented a new approach to apply the CELIV technique to organic semiconductor bilayer devices employing a polar electron transport layer, like Alq_3. The two sheet charge densities on either side of this polar layer lead to a shift of the hole injection voltage in the layer of interest to values lower than V_{bi}, zero or even negative bias. We take advantage of the fact that between this hole injection voltage and the built-in voltage the device behaves like a MIS-device, where the active layer is the semiconductor and the ETL takes the role of the insulator. Under these conditions, the MIS-CELIV experiment can be performed and the hole mobility of the active layer under investigation can be determined. This method therefore has the potential to be applied rather generally to new thin film semiconducting materials for organic solar cells and OLEDs. In combination with dipolar doping, both hole and electron mobility of a material can be assessed.

SUPPLEMENTARY MATERIAL

See supplementary material for the displacement current measurement (DCM) and the dark injection transient current (DITC) measurement, as well as the modeling parameters and simulated electric field profiles.

ACKNOWLEDGMENTS

We acknowledge financial support from the Swiss National Science Foundation (SNSF; Project No. 151563) and the Deutsche Forschungsgemeinschaft (DFG; Contract No. Br 1728/15-1) within the CARDYN Project. Furthermore, we

thank Dr. Neetu Chopra and Dr. Chris Brown from Kateeva Inc. for providing the single-layer hole-only α-NPD device used for the mobility determination by the DITC method reported in the supplementary material.

[1]J. C. Scott, S. Karg, and S. A. Carter, J. Appl. Phys. **82**, 1454 (1997).
[2]T. Tsutsui, E. Aminaka, C. P. Lin, and D. U. Kim, Philos. Trans. R. Soc. A **355**, 801 (1997).
[3]M. Regnat, S. Züfle, A. Gentsch, K. Pernstich, and B. Ruhstaller, "The importance of changes in the emission zone for the efficiency roll-off in OLEDS," Organic Electronics (unpublished).
[4]M. Kuik, G.-J. A. H. Wetzelaer, H. T. Nicolai, N. I. Craciun, D. M. D. Leeuw, and P. W. M. Blom, Adv. Mater. **26**, 512 (2014).
[5]W. Tress, A. Petrich, M. Hummert, M. Hein, K. Leo, and M. Riede, Appl. Phys. Lett. **98**, 063301 (2011).
[6]J. D. Kotlarski and P. W. M. Blom, Appl. Phys. Lett. **100**, 013306 (2012).
[7]M. M. Mandoc, L. J. A. Koster, and P. W. M. Blom, Appl. Phys. Lett. **90**, 133504 (2007).
[8]C. Deibel, A. Wagenpfahl, and V. Dyakonov, Phys. Status Solidi RRL **2**, 175 (2008).
[9]A. Armin, G. Juska, M. Ullah, M. Velusamy, P. L. Burn, P. Meredith, and A. Pivrikas, Adv. Energy Mater. **4**, 1300954 (2014).
[10]P. W. M. Blom, M. J. M. de Jong, and M. G. van Munster, Phys. Rev. B **55**, R656 (1997).
[11]K. S. Haber and A. C. Albrecht, J. Phys. Chem. **88**, 6025 (1984).
[12]M. Abkowitz and D. M. Pai, Philos. Mag. B **53**, 193 (1986).
[13]H. C. F. Martens, H. B. Brom, and P. W. M. Blom, Phys. Rev. B **60**, R8489 (1999).
[14]K. K. Tsung and S. K. So, J. Appl. Phys. **106**, 083710 (2009).
[15]P. A. Torpey, J. Appl. Phys. **56**, 2284 (1984).
[16]D. Poplavskyy, W. Su, and F. So, J. Appl. Phys. **98**, 014501 (2005).
[17]G. Horowitz, Adv. Mater. **10**, 365 (1998).
[18]G. Juška, K. Arlauskas, M. Viliūnas, and J. Kočka, Phys. Rev. Lett. **84**, 4946 (2000).
[19]A. Pivrikas, N. S. Sariciftci, G. Juška, and R. Österbacka, Prog. Photovoltaics **15**, 677 (2007).
[20]K. Genevicius, R. Österbacka, G. Juska, K. Arlauskas, and H. Stubb, Thin Solid Films **403–404**, 415 (2002).
[21]G. Juška, K. Arlauskas, M. Viliūnas, K. Genevicius, R. Österbacka, and H. Stubb, Phys. Rev. B **62**, R16235 (2000).
[22]A. Pivrikas, G. Juŝka, K. Arlauskas, M. Scharber, A. Mozer, N. Sariciftci, H. Stubb, and R. Österbacka, Proc. SPIE **5938**, 59380N (2005).
[23]M. Neukom, N. Reinke, and B. Ruhstaller, Sol. Energy **85**, 1250 (2011).
[24]S. Bange, M. Schubert, and D. Neher, Phys. Rev. B **81**, 035209 (2010).
[25]J. Lorrmann, B. H. Badada, O. Inganäs, V. Dyakonov, and C. Deibel, J. Appl. Phys. **108**, 113705 (2010).
[26]C. Deibel, Phys. Status Solidi A **206**, 2731–2736 (2009).
[27]S. A. Hawks, B. Y. Finck, and B. J. Schwartz, Phys. Rev. Appl. **3**, 044014 (2015).
[28]S. Jenatsch, R. Hany, A. C. Véron, M. Neukom, S. Züfle, A. Borgschulte, B. Ruhstaller, and F. Nüesch, J. Phys. Chem. C **118**, 17036 (2014).
[29]R. Häusermann, E. Knapp, M. Moos, N. A. Reinke, T. Flatz, and B. Ruhstaller, J. Appl. Phys. **106**, 104507 (2009).
[30]S. Züfle, M. T. Neukom, S. Altazin, M. Zinggeler, M. Chrapa, T. Offermans, and B. Ruhstaller, Adv. Energy Mater. **5**, 1500835 (2015).
[31]G. Juška, N. Nekrašas, and K. Genevicius, J. Non-Cryst. Solids **358**, 748 (2012).
[32]M. Nyman, O. Sandberg, J. F. M. Hardigree, S. Kola, H. E. Katz, and R. Österbacka, Appl. Phys. Lett. **103**, 243502 (2013).
[33]S. Berleb, W. Brütting, and G. Paasch, Org. Electron. **1**, 41 (2000).
[34]W. Brütting, S. Berleb, and A. G. Mückl, Org. Electron. **2**, 1 (2001).
[35]C. W. Tang and S. A. VanSlyke, Appl. Phys. Lett. **51**, 913 (1987).
[36]Y. Noguchi, Y. Miyazaki, Y. Tanaka, N. Sato, Y. Nakayama, T. D. Schmidt, W. Brütting, and H. Ishii, J. Appl. Phys. **111**, 114508 (2012).
[37]T. D. Schmidt, L. Jäger, Y. Noguchi, H. Ishii, and W. Brütting, J. Appl. Phys. **117**, 215502 (2015).
[38]S. Altazin, S. Züfle, E. Knapp, C. Kirsch, T. Schmidt, L. Jäger, Y. Noguchi, W. Brütting, and B. Ruhstaller, Org. Electron. **39**, 244 (2016).
[39]See www.fluxim.com for Paios - Platform for All-in-One Characterisation of Solar Cells, Fluxim AG, 2016.
[40]See www.fluxim.com for Setfos 4.4, Fluxim AG, 2016.
[41]M. Neukom, S. Züfle, and B. Ruhstaller, Org. Electron. **13**, 2910 (2012).
[42]B. Ruhstaller, E. Knapp, B. Perucco, N. Reinke, D. Rezzonico, and F. Müller, in *Optoelectronic Devices and Properties* (InTech, 2011), Chap. 21.
[43]E. Knapp and B. Ruhstaller, J. Appl. Phys. **117**, 135501 (2015).
[44]H. Okumoto and T. Tsutsui, Appl. Phys. Express **7**, 061601 (2014).
[45]S. Egusa, A. Miura, N. Gemma, and M. Azuma, Jpn. J. Appl. Phys. **33**, 2741 (1994).
[46]J. Važgėla, K. Genevičius, and G. Juška, Chem. Phys. **478**, 126 (2016).
[47]Z. Deng, S. Lee, D. Webb, Y. Chan, and W. Gambling, Synth. Met. **107**, 107 (1999).
[48]E. W. Forsythe, M. A. Abkowitz, Y. Gao, and C. W. Tang, J. Vac. Sci. Technol. A **18**, 1869 (2000).
[49]S. Naka, H. Okada, H. Onnagawa, Y. Yamaguchi, and T. Tsutsui, Synth. Met. **111–112**, 331 (2000).
[50]A. Fleissner, H. Schmid, C. Melzer, and H. von Seggern, Appl. Phys. Lett. **91**, 242103 (2007).
[51]K. L. Tong, S. W. Tsang, K. K. Tsung, S. C. Tse, and S. K. So, J. Appl. Phys. **102**, 093705 (2007).
[52]C. Lin, Y. Chen, H. Chen, F. Fang, Y. Lin, W. Hung, K. Wong, R. Kwong, and S. Xia, Org. Electron. **10**, 181 (2009).
[53]N. D. Nguyen, M. Schmeits, and H. P. Loebl, Phys. Rev. B **75**, 075307 (2007).
[54]T. Matsushima, Y. Kinoshita, and H. Murata, Appl. Phys. Lett. **91**, 253504 (2007).
[55]T. Matsushima and C. Adachi, Thin Solid Films **517**, 874 (2008).
[56]L. Jäger, T. D. Schmidt, and W. Brütting, AIP Adv. **6**, 095220 (2016).
[57]Y. Noguchi, H. Lim, T. Isoshima, E. Ito, M. Hara, W. Won Chin, J. Wook Han, H. Kinjo, Y. Ozawa, Y. Nakayama, and H. Ishii, Appl. Phys. Lett. **102**, 203306 (2013).
[58]D. Y. Kondakov, J. R. Sandifer, C. W. Tang, and R. H. Young, J. Appl. Phys. **93**, 1108 (2003).
[59]Y. Noguchi, N. Sato, Y. Tanaka, Y. Nakayama, and H. Ishii, Appl. Phys. Lett. **92**, 203306 (2008).
[60]E. Ito, Y. Washizu, N. Hayashi, H. Ishii, N. Matsuie, K. Tsuboi, Y. Ouchi, Y. Harima, K. Yamashita, and K. Seki, J. Appl. Phys. **92**, 7306 (2002).